Brazilian Journal
of Chemical
Engineering

ISSN 0104-6632
Printed in Brazil
www.abeq.org.br/bjche

Vol. 36, No. 03, pp. 1333 - 1342, July - September, 2019
dx.doi.org/10.1590/0104-6632.20190363s20180478

INVESTIGATION OF THE EFFECT OF ELECTRIC FIELD ON CO_2 ABSORPTION IN WATER/Fe_3O_4 NANOFLUID

N. Hoseini[1], M. Nasr Esfahany[1*], N. Etesami[1], Hajar Taheri Afarani[2] and E. Fadaie[1]

[1] Isfahan University of Technology, Department of Chemical Engineering, Isfahan, Iran. ORCID: 0000-0001-9067-2529;
E-mail: mnasr@cc.iut.ac.ir - ORCID: 0000-0003-4475-7075; ORCID: 0000-0002-4370-1566; ORCID: 0000-0001-6570-1666
[2] Tennessee Technological University, Department of Chemical Engineering, Cookeville, United States. ORCID: 0000-0001-7959-1453

(Submitted: October 15, 2018 ; Revised: February 16, 2019 ; Accepted: February 20, 2019)

Abstract - In this study, a novel strategy for controlling the mass transfer rate in a gas-liquid system was reported and used for the industrially important system of CO_2 absorption. The strategy used Fe_3O_4 nanoparticles in the liquid phase and also exerting an external electric field. To demonstrate this approach, a unique experimental set up was applied to form a falling liquid film, which was water, to be in contact with the gas phase, which was pure carbon dioxide. Nanofluid with concentrations less than 0.03% by volume and field intensities of 133, 200, 266 kV/m were used in this study. Experimental results showed that the external electric field was able to remarkably enhance the gas absorption rate in dilute nanofluids, while it deteriorated mass transfer in concentrated nanofluids. In order to explain the results, the viscosity of the nanofluid was also experimentally measured in the presence of the electric field.
Keywords: Mass transfer; Electric field; Nanofluid.

INTRODUCTION

Gas absorption into the liquid phase is a process of considerable industrial importance and has many applications. Gas dehydration and selective absorption of H_2S in the gas industry, hydrocarbon absorbers for lean oil in refineries, and Ethylene Oxide absorption in the petrochemical industry are some examples of it. This process is defined as contacting a gas mixture with a liquid for the goal of dissolving one or more components of the gas in the liquid phase (Treybal, 2001).

Enhancement methods can be used to decrease the absorption process costs significantly. Generally, these methods are divided into two main categories: Active and inactive methods. No external force is used in inactive methods while in active methods an external force is directly exerted on the system (Laohalertdecha et al., 2007). Inactive methods include mechanical and chemical methods and the use of nanoparticles. Mechanical methods improve performance by modifying the shape, surface, and structure of the absorption equipment. Chemical methods improve absorption performance by adding additives and surfactants to the solution. The word nanofluid was used first by Choi (1995) to introduce suspensions containing particles with sizes less than 100 nm. There are several studies considering the effects of nanoparticles on heat transfer (Lee et al., 1999;, Heris et al., 2007;, Mansour et al., 2007; Heris et al., 2006a;, Das et al., 2003;, Hwang et al., 2009; Pak and Cho, 1998;, Heris et al., 2006b; Xuan, 2003; Xuan and Roetzel, 2000) but published reports dealing with nanoparticle effects on mass transfer are scarce.

In a study the literature on mass transfer in nanofluids in two different sections of mass diffusivity and convective mass transfer summarized by Ashrafmansouri and Nasr Esfahany (2014). Beiki et al. (2013) investigated the mass transfer of ferricyanide ions through electrolyte nanofluids in a circular

* Corresponding author: M. Nasr Esfahany - E-mail: mnasr@cc.iut.ac.ir

tube experimentally. Nanofluids consisted of 40 nm γ-Al_2O_3 nanoparticles suspended in ferri-ferrocyanide and aqueous sodium hydroxide as the base fluid. Measurements showed that the mass transfer coefficient increased with the concentration of Nanofluid up to 0.01%. For greater concentrations of nanoparticles in the nanofluid, the mass transfer coefficient decreased with the concentration. Absorption of hydrogen sulfide and carbon dioxide in exfoliated graphene oxide (EGO)-water and synthesized silica (SS)-water nanofluids in a bubble column was investigated experimentally by Esmaeili-Faraj and Nasr Esfahany (2016). Due to the adsorption of H_2S by Oxygen group functionalities and silanol groups in EGO and SS nanoparticles, the mass transfer coefficient, K_L, increased more than 500% and 200% relative to the based fluid, respectively. In another study, effect of silica nanoparticles on mass transfer was studied in a circular tube by using an electrochemical limiting current technique in both laminar and turbulent flow regimes. The base fluid was composed of equimolar potassium ferri-ferrocyanide and sodium hydroxide. Measurements for the laminar regime indicated that the mass transfer coefficient increased with nanofluid volume fraction up to 0.0057% and decreased with increasing the volume fraction of nanoparticles further. In the turbulent flow regime, no enhancement was recognized due to the addition of silica nanoparticles to the base electrolyte solution (Keshishian et al., 2013). Darvanjooghi et al. (2018) investigated the effect of nanoparticle size on diffusion coefficient, renewal surface rate, and thickness of diffusion layer within the liquid in silica/water nanofluid. Their obtained results showed that by the increment of nanoparticle size, the renewal surface rate increased while diffusivity and liquid film thickness decreased. Consequently, the mass transfer coefficient of carbon dioxide increased by the increment of nanoparticle size.

As mentioned previously, the active method is another category of enhancement method. In the active method, an external force is exerted on the system. This external force can be created by an external field. To illustrate, the magnetic nanoparticle effect on mass transfer in an external alternating magnetic field was studied (Suresh and Bhalerao, 2001). A 40-50% increase in absorption rate was observed in both bubble and wet wall columns. Furthermore, the effect of Fe_3O_4 nanoparticles on the absorption of carbon dioxide into methyl diethanol amine (MDEA) solution in a wet wall column was investigated (Komati and Suresh, 2008). The results showed that the enhancement in volumetric mass transfer coefficient increases with the volume fraction of solid magnetite in the presence of a magnetic field. Moreover, the effects of upward and downward magnetic field on Ammonia/Water falling film absorption in a wet wall column were studied (Niu et al., 2010). According to the results, mass and heat absorption in downward (upward) magnetic fields are higher (lower) than those in the absence of magnetic fields. By using a different geometry, the effect of alternating magnetic field on suspended magnetic particles in a stirred tank was investigated (Reichert et al., 2004). Stirrer speed and magnetic field intensity were the main variables studied. Up to 200% augmentation in the mass transfer coefficient on the liquid side was attained in experiments.

Another example of the active method is applying an external electric field. AC electrokinetic (ACEK) effects, including dielectrophoresis (DEP), AC electroosmosis (ACEO), and AC electrothermal (ACET) effects are increasingly applied in microfluidic devices to manipulate fluids and embedded particles (Cheng, 2017). DEP directly acts on the particles suspended in the fluid, while ACEO and ACET effects cause fluid movements that carry the particles. Cheng investigated the development of a low-cost biosensing platform that can be used for viral disease diagnosis and chemical detection (Cheng, 2017). The sensing mechanism was known as AC electrokinetic (ACEK) capacitive sensing. By applying an inhomogeneous AC electric field on sensor electrodes, positive dielectrophoresis is induced to accelerate the travel of analytes. Elder et al. (2004) described theories and physics behind AC electrokinetics focusing on dielectrophoresis, electrorotation, and traveling wave dielectrophoresis and then mentioned techniques for making devices which actualize these theories and are very diverse in use. Park and Lu (2007) investigated induced torque and orientation of core-shell nanoparticles in an electric field. They showed that the shell of a nanoparticle has an important effect on its orientation. Besides the shell, they mentioned that permittivity, conductivity, and field frequency together determine the magnitude and direction of the induced torque. In another study, orders of magnitude of the various forces experienced by a sub-micrometer latex particle in a model electrode structure were calculated by Ramos et al. (1998), and results were compared with the experiment. They described the relative influence of each type of force on the overall behavior of particles (Ramos and et al., 1998). Majazi Dalfard (2012) investigated AC electric field deposition behavior of TiO_2 ceramic nanoparticles at different applied frequencies. The results by scanning electron microscopy (SEM) showed that by increasing frequency from 1 to 10000 Hz, the deposition mechanism of TiO_2 particles of the surface of gold electrodes changes. He also mentioned that this technique is capable of controlling the deposition pattern and manipulating nanoparticles. Modarres and Tabrizian (2017) provided a concise overview of the theory behind AC electroosmosis

and AC electrothermal flows and pointed out key parameters for consideration and optimization. They further summarized experimental techniques for dielectrophoresis of the two most extensively studied biomacromolecules, DNA and protein molecules, and elaborated on their potential applications in separation, and mass transport for biosensing devices.

Experimental data considering the effects of external electric fields on mass transfer in nanofluids, which have profound applications in the industry, do not exist. The present study is motivated by this lack of data. The objective of the present work is the investigation of the effects of an electric field on mass transfer in a Fe_3O_4/Water nanofluid.

EXPERIMENTAL SET-UP

A schematic of the experimental set-up used in this study is shown in Figure 1. It consisted of a wooden frame for holding tubes vertically (1), vertical plastic tubes with two different inner diameters of 6 and 14 mm all with length of 50 cm (2), two copper electrodes for exerting the electric field, 28 cm in height and 6 cm in width, 7.5 cm apart (3), an entrance section (4) and exit section (5). A multimeter (model HIOKI/3010 Japan) was used for measuring the voltage between two electrodes with an uncertainty of ±0.5kV (6). A high voltage power supply was used to impose an electric field (7). Two digital cameras were fixed at the entrance and exit section of the tube 30 cm apart for taking photos (8). The breaking voltage for the explained geometry was measured to be about 25 kV. Experiments were performed at room pressure and temperature. Barometric pressure was measured with a mercury barometer accurate to ±0.05cm Hg (~67 Pa). The temperature of the test fluid was measured by a thermometer accurate to ±0.5 ºC. The time required for the bubble to pass the distance between cameras was measured by a stopwatch accurate to 0.01s. Length of the bubble at the entrance and exit sections and height of liquid that was above the gas bubble at the exit section were measured by means of photographs using Adobe Photoshop software, all with an uncertainty of ±0.0005m.

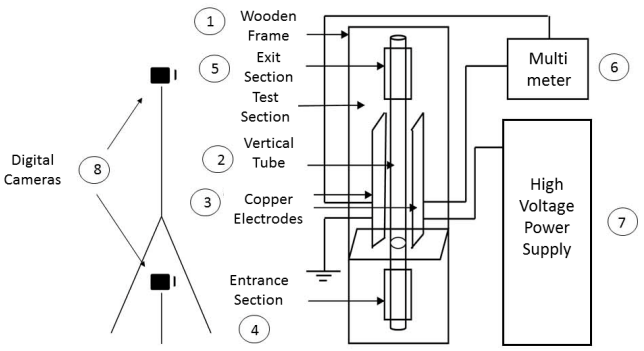

Figure1. Experimental set up: 1 - Wooden frame; 2 - Vertical tube; 3 - Copper electrodes; 4 - Entrance section; 5 - Exit section; 6 - Multimeter; 7 - High voltage power supply; 8 - Digital cameras.

MATERIALS

Carbon dioxide 99.9% pure in a reservoir was used as the gas phase. Nanofluid was purchased from Plasmachem (GmbH Rudower Chaussee 29, 12489 Berlin) in a stable concentrated suspension and diluted to three different concentrations (0.001%, 0.01% and 0.025% by volume) by adding base fluid (double-distilled water) to the suspension. The diluted suspension was stable and no sign of sedimentation was observed in stagnant nanofluid after months. The physical properties of the nanofluid are shown in Table1. A TEM image of the nanosuspension used in this work is shown in Figure 2

Table1. Physical properties of the nanosuspension of magnetic particles.

Concentration	7 vol.%
Nanosized particles	Fe_3O_4
Mean diameter (nm)	8
Stabilizer	oleic acid (3%)
Particle density (kg/m^3)	4950

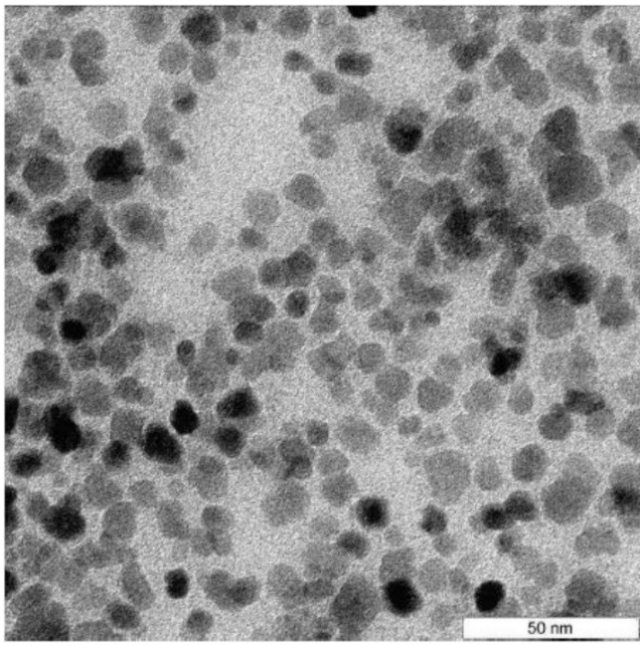

Figure 2. Transmission Electron Microscopy (TEM) of 7 % nanofluid.

EXPERIMENTAL PROCEDURE

A vertical plastic tube was first filled by liquid. An external electric field was imposed by electrodes connected to the high voltage power supply. Three voltages of 10, 15 and 20 kV were used in the

experiments. 5 ml of gas was injected at the bottom of the test tube by means of a syringe. The gas bubble moved upward in the tube and a liquid falling film formed on the tube wall. Figure 3 shows schematically the falling film surrounding the rising bubble.

The length of the bubble reduced while rising due to absorption into the liquid phase. The length change of the bubble was recorded by taking photographs at the entrance and exit sections of the test tube. Experiments were performed with base fluid and nanofluids both in the absence and presence of the electric field. Every run was repeated at least three times. Regeneration of used nanofluid was performed by means of nitrogen bubbling through the liquid. The pH was used as an indication of complete regeneration of the nanofluid. Nitrogen bubbling continued through the liquid until the fresh nanofluid pH was achieved. Reduction of bubble length is shown in Figure 4.

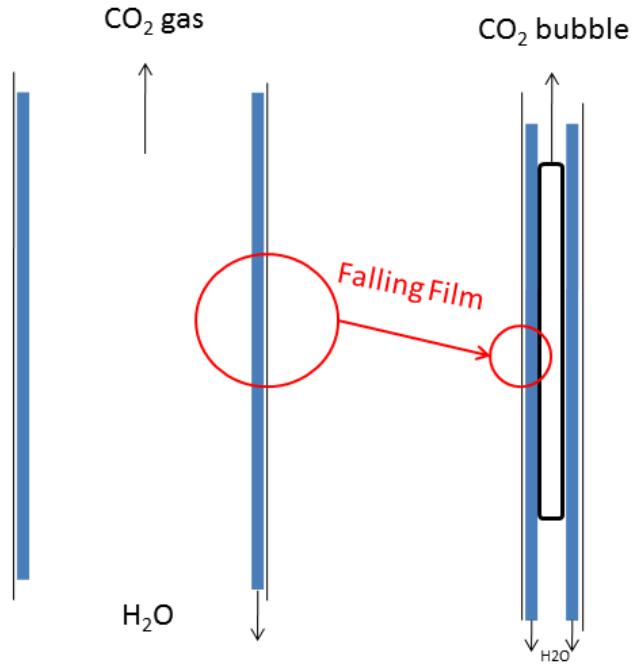

Figure 3. Falling film surrounding the rising bubble.

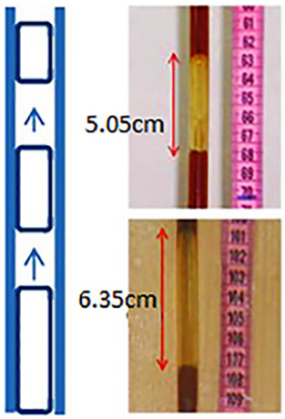

Figure 4. Reduction of rising bubble length in the 6 mm diameter tube filled with 0.01% nanofluid.

DATA PROCESSING

In order to calculate the mass transfer coefficient, CO_2 mass balance was written for a rising bubble:

$$-2N\pi RLM_{CO_2} = \frac{dm}{dt} = \rho_{CO_2}\frac{dV}{dt} = \rho_{CO_2}\pi R^2\frac{dL}{dt} \quad (1)$$

In the above equation, N is the molar flux of CO_2 in (kmol/m^2.s), π is pi number, R is the tube radius in (m), L is the bubble length in (m), M_{CO2} is the molecular weight of carbon dioxide in (kg/kg.mol), m is mass in (kg), t is time in (s), V is the volume of gas bubble in (m^3), and ρ_{CO2} is the density of carbon dioxide in (kg/m^3). In equation (1) transfer from the bottom and top caps of the bubble was considered to be negligible compared to the transfer from the periphery. N, the molar flux of CO_2 (kmol/m^2. s), is derived by multiplying the mass transfer coefficient by the driving force (Treybal, 2001), which is CO_2 concentration difference (ΔC) between bubble surface and the bulk of the liquid. If an equilibrium state can be considered between gas and liquid on the bubble surface (interface of two phases), CO_2 concentration on the bubble surface will be equal to the solubility of CO_2 in water at 25°C, C_i (kmol/m^3), and in the bulk of the liquid will be zero:

$$N = k_{exp.}\Delta C = k_{exp.}C_i \quad (2)$$

In equation (2), $k_{exp.}$ is the experimental mass transfer coefficient in (m/s). The density of CO_2 is a function of pressure. The height of liquid above the bubble changes while the bubble rises through the tube, causing a change in pressure and consequently density. Assuming that CO_2 is an ideal gas, the density of the rising bubble can be written as:

$$\rho_{CO_2} = \frac{PM_{CO_2}}{TR_g} = \frac{M_{CO_2}}{TR_g}\left[P_{ambient} + \rho_f g\left(h' + h - \bar{u}t\right)\right] \quad (3)$$

In equation (3), P is pressure in (Pa), T is temperature in (K), R_g is the gas constant in (J/kmol.K), g is gravity acceleration in (m^2/s), ρ_f is fluid density in (kg/m^3), h$'$ is the height of liquid above the bubble at the exit section in (m), and h and $\bar{u}$ are path length in (m) and average bubble velocity in (m/s), respectively. By placing equations (2) and (3) into equation (1), after simplification and integration, the experimental mass transfer coefficient is derived:

$$k_{exp.} = \frac{\rho_f gR\bar{u}\ln\left(\frac{L_2}{L_1}\right)}{2R_g TC_i \ln\left(\frac{P_{ambient} + \rho_f g\left(h' + h - \bar{u}t\right)}{P_{ambient} + \rho_f g\left(h' + h\right)}\right)} \quad (4)$$

In the above equation, L_1 and L_2 are the length of bubble in (m) at the entrance and exit sections of the tube, respectively. An average value for bubble velocity is used in the above equation by dividing the path length by time. End effects are also neglected. Experimental Sherwood number is defined as:

$$\mathrm{Sh(exp.)} = \frac{k(\mathrm{exp.})\delta}{D} \tag{5}$$

In equation (5), δ and D are falling film thickness in (m) and diffusion coefficient in (m^2/s), respectively. The liquid film around the rising bubble can be assumed as a falling film. The volumetric flow rate of falling liquid can be calculated from the volumetric flow rate of the rising gas bubble. Multiplying the volumetric flow rate of the falling film by liquid density gives the mass flow rate of the liquid. Mass flow rate per unit length, Γ, in (kg/m.s) is calculated by equation (6) (Treybal, 2001) in which d in (m) is tube diameter. Reynolds number, Re, for the falling film is calculated by equation (7) (Treybal, 2001). μ_f is fluid viscosity in (Pa.s).

$$\Gamma = \frac{\frac{\pi}{4}d^2\bar{u}\rho_f}{\pi d} = \frac{d\bar{u}\rho_f}{4} \tag{6}$$

$$\mathrm{Re} = \frac{4\Gamma}{\mu_f} \tag{7}$$

The thickness of the falling film surrounding the rising bubble, δ in (m), can be estimated by equation (8) (Treybal, 2001).

$$\delta = \left(\frac{3\bar{u}\mu_f}{\rho_f g}\right)^{0.5} \tag{8}$$

The theoretical Sherwood number, $Sh_{th.}$, for a falling film is correlated with the Reynolds (Re) and Schmit (Sc) numbers as shown in equation (9) and (10) (Treybal, 2001). Schmit number is defined as the ratio of kinematic viscosity to diffusion coefficient and can be extracted from Treybal (2001) for water. Reynolds number in equations (9) and (10) can be calculated by using equations (6) and (7). As mentioned before, an average value for bubble velocity is assumed and used in equation (6) by dividing the path length by time. Theoretical mass transfer coefficient, $k_{th.}$ in (m/s), can be calculated from the Sherwood number by equation (11) (Treybal, 2001),

$$\mathrm{Sh(th.)} = \left(\frac{3}{2\pi}\frac{\delta}{L}\mathrm{ReSc}\right)^{0.5} \quad (100 < \mathrm{Re} < 1200) \tag{9}$$

$$\mathrm{Sh(th.)} = \left(1.76\times10^{-5}\right)\mathrm{Re}^{1.506}\,\mathrm{Sc}^{0.5} \quad (\mathrm{Re} > 1200) \tag{10}$$

$$k(\mathrm{th.}) = \frac{\mathrm{Sh(th.)}D}{\delta} \tag{11}$$

Physical properties of the nanofluid were calculated by the following equations (Yu and Choi, 2003; Joensson et al., 1986):

$$\rho_{nf} = (1-\varphi)\rho_f + \varphi\rho_p \tag{12}$$

$$\mu_{nf} = \mu_f(1+2.5\varphi) \tag{13}$$

All physical properties were calculated at the bulk temperature of the liquid.

RESULTS AND DISCUSSION

Mass transfer coefficient measurement: Base fluid

The accuracy of the experimental setup and procedure was first checked by a set of experiments with water as the base fluid in the absence of an electric field and nanoparticle. Theoretical and experimental Sherwood numbers were calculated by equations (9) and (10) and (5) for the base fluid. A constant value of 1.96E-9 m^2/s [(Treybal, 2001)] was assumed and used for the diffusion coefficient of CO_2 in water for calculating theoretical and experimental Sherwood numbers based on equations (9), (10), and (5). The thickness of the falling film, δ, in equations (5) and (9) was calculated by equation (8). Figure 5 shows a comparison between experimental and theoretical results. The maximum deviation is 0.45 %.

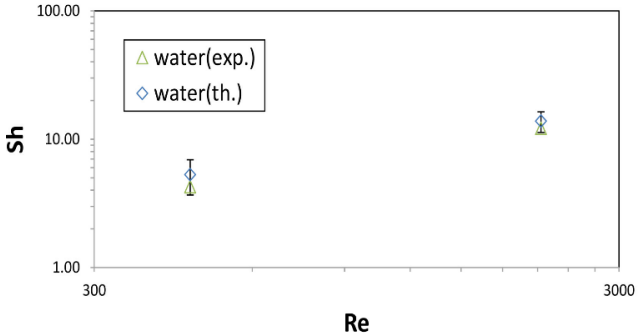

Figure 5. Comparison of experimental Sherwood number with predictions by equations (9) and (10).

Mass transfer coefficient measurement: Nanofluids

To investigate the effects of an electric field on mass transfer in nanofluids, experiments were performed with nanofluids in three different concentrations both in presence and absence of an electric field. The ratios of experimental mass transfer coefficient in the electric field to that in the absence of field (calculated

by equation (4)) versus applied voltages for different nanofluid concentrations and different tube diameters are plotted in Figure 6 and 7. Since Reynolds number for flow transition from laminar to turbulent flow regime in the current experimental system is 1200 (Treybal, 2001), two different diameters were considered in the experiments so that both laminar (d=6mm, Re= 460) and turbulent (d=14 mm, Re=2100) flow regimes were taken into account under the experimental conditions. Experimental uncertainty in the relative mass transfer coefficient was calculated following the method illustrated in (Kline and McClintock, 1953) and is less than 16%.

Figure 6 shows that exerting an electric field leads to an increased mass transfer rate in nanofluid of 0.001% concentration, and increasing field intensity improves mass transfer augmentation while a different behavior is observed at two other nanofluid concentrations in the same experimental conditions. For nanofluid with 0.01% and 0.025% concentrations, exerting an electric field results in a decreasing mass transfer rate. A similar trend is also observed in Reynolds number of 2100 which is shown in Figure 7.

All nanofluids used in this study consisted of double-distilled water as medium and Fe_3O_4 as embedded

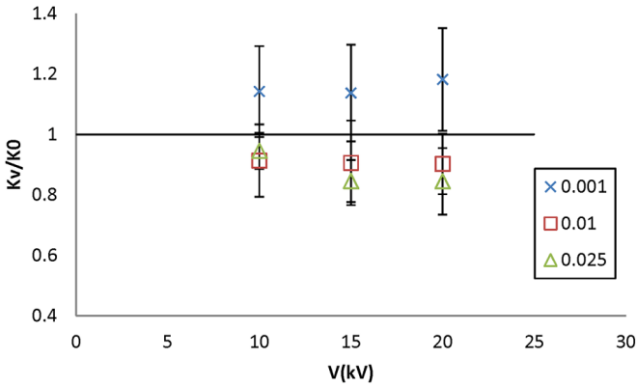

Figure 6. Effect of electric field on the mass transfer coefficient at different nanofluid concentrations for Re = 460.

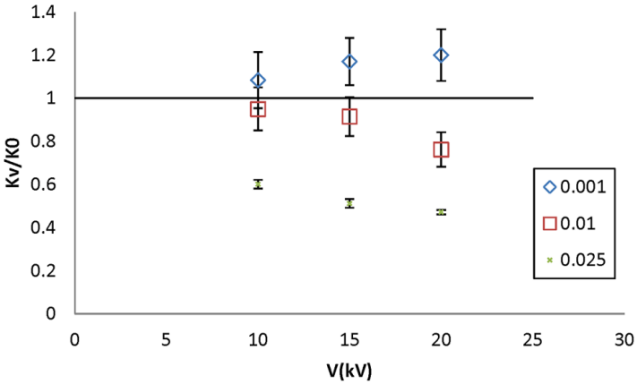

Figure 7. Effect of electric field on the mass transfer coefficient in different nanofluid concentrations for Re = 2100.

particles. When nanoparticles are suspended in a non-uniform electric field, the applied field induces a dipole inside the particles (Elder et al., 2004). The interaction between the non-uniform field and the induced dipole generates a force called dielectrophoresis (DEP). If the particles are more conductive than the medium, the dipole aligns with the field, causing attraction of particles to the surface of the electrode (positive DEP force) and if the medium is more conductive than the particles, the induced dipole aligns against the field, causing repulsion of the particles from the surface of the electrode (negative DEP force). According to Bagheliet al. (2015), the electrical conductivity of Fe_3O_4 nanoparticles is much larger than that of base fluid. Hence, positive DEP force causes nanoparticles to be attracted towards the surface of the electrode and aligned with the field. This alignment may lead to chain formation of the particles, and consequently, increased viscosity of the nanofluid under the electric field, which results in increased falling film thickness which follows with decreased mass transfer rate according to equations (8) and (11), respectively. Afore-mentioned descriptions reasonably explain the behaviors observed for 0.01% and 0.025% nanofluid concentrations under the applied field intensities.

For confirmation, the viscosity of nanofluids in three different concentrations under the applied voltages was experimentally measured. A capillary tube viscometer with an inner diameter of 1 mm and length of 30 cm as discussed in Rarani et al. (2012) was used to measure the viscosity of nanofluids. Electrodes were placed around the capillary tube in the viscometer in order to impose the electric field. Figure 8 compares the measured viscosity of nanofluids with predictions by equation (13) (Einstein model). Each measurement was repeated at least three times and the standard deviation of the measurements was plotted as error bars.

It can be seen that measured viscosities are greater than predictions by equation (13). In other words, equation (13) underpredicts the viscosity by 1.7% on average. Lee et al. (2008) also reported that viscosity of nanofluids is greater than that predicted viscosities

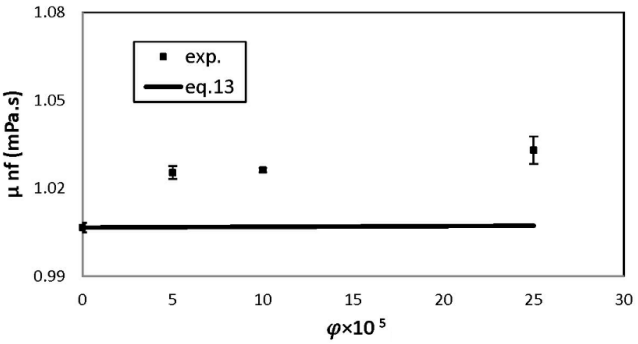

Figure 8. Viscosity of nanofluids versus nanoparticle volume fraction.

by equation (13). In another study, Duangthongsuk and Wongwises (2009) reported that the viscosity of H_2O/TiO_2 nanofluid is 11% higher than those calculated by equation (13).

Figure 9 shows relative viscosity (ratio of viscosity in the electric field to that in the absence of field) versus voltage between two electrodes. The standard deviation of relative viscosities measured was less than 0.6%. As Figure 9 shows, the viscosity of the base fluid decreases with imposed voltages. The increasing voltage between two electrodes decreases the relative viscosity of water. Exerting electric field has an opposite effect on the viscosity of nanofluids. Nanofluid viscosity increases under the electric field. The relative viscosity of nanofluids increases with electric field intensity. Bloodworth and Wendt (1995) and Hasley (1992) reported an increase of suspension viscosity due to exerting an electric field. They attributed this effect to the chain formation of the particles in the suspension induced by their polarization in the electric field.

There might be a different scenario for the nanofluid with a concentration of 0.001% under applied field since, as Figures 6 and 7 show, the electric field has increased the mass transfer rate in this nanofluid. The AC electroosmosis effect can induce microfluidic vortices in dilute suspensions and then accelerates the movement of target molecules and improve the mass transfer rate (Cheng, 2017). As mentioned previously, when nanoparticles are suspended in a non-uniform electric field, the applied field induces a dipole inside the particle (Elder et al., 2004). In other words, positive and negative charges appear in the Fe_3O_4 nanoparticles. AC electroosmosis flow is caused by movement of induced charges and consequently Fe_3O_4 nanoparticles, which carry these charges in the electrical double layer (EDL) at the solid-liquid interface (Cheng, 2017). The EDL is a structure that appears on the surface of an object (electrodes in this study) when it is exposed to a fluid (Delgado et al., 2005). The EDL refers to two parallel layers of the charge surrounding the electrode. The first layer, the surface charge (either positive or negative), consists of ions adsorbed onto the electrodes, and the second layer is composed of ions attracted to the surface charge via the Coulomb force, electrically screening the first layer. The induced counter-ions will move under the electric field to generate ACEO flows (Elder et al., 2004). The flow velocity of AC electroosmosis has been observed to decrease significantly with increasing conductivity. Accordingly, the AC electroosmosis effect is more significant in the 0.001% nanofluid compared to 0.01% and 0.025% nanofluids since the nanofluid with 0.001% concentration has lower conductivity than 0.01% and 0.025% nanofluids (Bagheli et al., 2015). It seems that AC electroosmosis flow weakens the effect of positive DEP, which results in increased viscosity in nanofluid of 0.001% concentration. As can also be seen in Figure 9, the amount of increase in the viscosity of the nanofluid of 0.001% is less than the amount of increase in viscosity of the other two nanofluid concentrations, which implies the existence of more significant AC electroosmotic flow in the 0.001% nanofluid. Similar studies have described systems and methods for manipulating particle behavior using the AC electrokinetic technique. Sin et al. (2009) proposed a hybrid electrokinetic manipulation system in which the combination of dielectrophoresis and AC electrothermal flow allows separation, mixing and concentration of colloidal particles ranging from nanometers to micrometers. Furthermore, Goa and et al. (2011, 2012) demonstrated a 3-parallel-electrode configuration for continuous isolation of various bacteria and mammalian cells. By correctly designing the channel and operating conditions, they demonstrated that AC electrothermal flow constraints target cells far away from the bulk solution toward the electrode surface, where DEP is most effective.

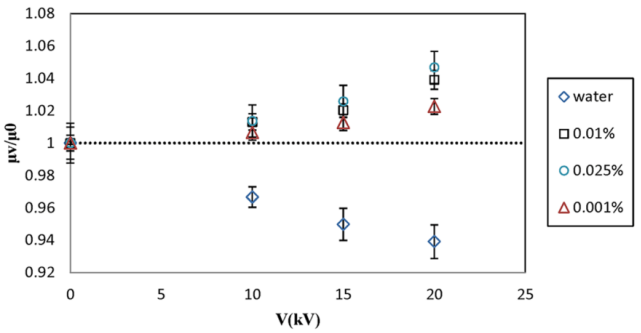

Figure 9. Effect of electric field on the viscosity of base fluid and nanofluids.

CONCLUSIONS

The mass transfer coefficient of CO_2 absorption in Fe_3O_4/Water nanofluid was experimentally measured under an external electric field. The obtained results showed improvement in the mass transfer coefficient of nanofluid under the electric field when the concentration was 0.001%, while in two other nanofluid concentrations (0.01% and 0.025%), a reduction trend was observed. Positive DEP leads to aligning the induced dipole inside nanoparticles with the electric field and trapping them in the nearest distance from the electrodes, causing attraction which results in increased viscosity. This behavior was confirmed by experimental measurement of nanofluid viscosity under the electric field. Augmentation of the mass transfer rate in the nanofluid of 0.001% seems to be due to vortices caused by the AC electroosmosis effect,

which leads to the movement of Fe_3O_4 nanoparticles trapped by DEP force.

It is anticipated that recent technological advances in AC electrokinetics, including dielectrophoresis and electrohydrodynamic fluid movement, could be applied to develop new methods and systems for characterization, manipulation, and control of nano-sized particles.

NOMENCLATURE

C	Molar concentration (kmol/m^3)
D	Diffusion coefficient (m^2/s)
d	Tube diameter (m)
g	Gravity acceleration (9.8 m^2/s)
h	Path length (m)
h'	Height of liquid above the bubble at exit section (m)
k (exp.)	Experimental mass transfer coefficient (m/s)
k (th.)	Theoretical mass transfer coefficient (m/s)
L	Length of the bubble (m)
m	Mass (kg)
N	Molar flux (kmol/m^2.s)
P	Pressure (Pa)
Sh (th.)	Theoretical Sherwood number
Re	Reynolds number
Sc	Schmit number
M	Molecular weight (kg/kg.mol)
R	Tube radius (m)
Rg	Gas constant (J/Kmol.K)
Sh(exp.)	Experimental Sherwood number
t	Time (s)
T	Temperature of the fluid (K)
$\bar{U}$	Average velocity of the gas bubble (m/s)
V	Volume of gas bubble (m^3)

Greek Letters

δ	Falling film thickness (m)
Γ	Mass of liquid flow per unit of film width (kg/m.s)
μ	Viscosity (Pa.s)
ρ	Density (kg/m^3)
φ	Nanoparticle volume fraction
Δ	Difference
π	Pi number, constant

Subscripts

i	Interface
CO_2	Carbon dioxide
1	Entrance section of tube
2	Exit section of tube
P	Particle
V	Presence of field
o	Absence of field
f	Fluid
nf	Nanofluid

REFERENCES

Ashrafmansouri, S.-S., Nasr Esfahany, M. Mass transfer in nanofluids: A review. International Journal of Thermal Sciences, 82, 84-99 (2014). https://doi.org/10.1016/j.ijthermalsci.2014.03.017

Bagheli, S., Khandan Fadafan, H., Lotfi Orimi, R., Ghaemi, M. Synthesis and Experimental Investigation of The Electrical Conductivity of Water-Based Magnetite Nanofluids. Powder Technology, 274, 426-430 (2015). https://doi.org/10.1016/j.powtec.2015.01.050

Beiki, H., Nasr Esfahany, M., Etesami, N. Laminar Forced Convective Mass Transfer of γ-Al $_2O_3$/ Electrolyte Nanofluid in a Circular Tube. International Journal of Thermal Sciences, 64, 251-256 (2013). https://doi.org/10.1016/j.ijthermalsci.2012.09.004

Bloodworth, R., Wendt, E. Materials for ER Fluids, Proceedings of the 5th International Conference on ER Fluids, MR Suspensions and Applications, World Scientific, 118-131(1995).

Cheng, C. Development of a Low-Cost biosensing platform for highly sensitive and specific on-site detection of pathogens and infections. Ph.D. Thesis, University of Tennessee, USA (2017).

Choi, S.U.S. Enhancing Thermal Conductivity of Fluids with Nanoparticles, Developments, and Applications of Non-Newtonian Flows FED, 66, 99-105 (1995).

Darvanjooghi, M.H.K., Esfahany, M.N., Esmaeili-Faraj, S.H. Investigation of the effects of nanoparticle size onCO2 absorption by silica-water nanofluid. Separation and Purification Technology, 195, 208-215 (2018). https://doi.org/10.1016/j.seppur.2017.12.020

Das, S.K., Putra, N., Thiesen, P., Roetzel, W. Temperature Dependence of Thermal Conductivity Enhancement for Nanofluids. Journal of Heat Transfer, 125, 567-574 (2003). https://doi.org/10.1115/1.1571080

Delgado, A.V., Gonzalez-Caballero, F., Hunter, R.J., Koopal, L.K., Lyklema, J. Measurement and Interpretation of Electrokinetic Phenomena. International Union of Pure and Applied Chemistry, 77, 1753-1805 (2005). https://doi.org/10.1351/pac200577101753

Duangthongsuk, W., Wongwises, S. Measurement of Temperature-Dependent Thermal Conductivity and Viscosity of TiO2/Water Nanofluids. Experimental Thermal, and Fluid Science, 33, 706-714 (2009). https://doi.org/10.1016/j.expthermflusci.2009.01.005

Elder, S., Gathright, W., Levy, B., Tu, W. AC Electrokinetics and Nanotechnology Meeting the Needs of the Room at the Bottom, (2004).

Esmaeili-Faraj, S.H., Nasr Esfahany, M. Absorption of Hydrogen Sulfide and Carbon Dioxide in Water BasedNanofluids. Industrial and Engineering Chemistry Research, 55, 4682-4690 (2016). https://doi.org/10.1021/acs.iecr.5b04816

Gao, J., Riahi, R., Sin, M.L.Y., Zhang, S.F., Wong, P.K., Electrokinetic Focusing, and Separation of Mammalian Cells in Conductive Biological Fluids. Analyst, 137, 5215-5221 (2012). https://doi.org/10.1039/c2an35707k

Gao, J., Sin, M.L., Liu, T., Gau, V., Liao, J.C., Wong, P.K. Hybrid electrokinetic manipulation in high-conductivity media. Lab on a Chip, 11, 1770-1775 (2011). https://doi.org/10.1039/c1lc20054b

Hasley, T.C. Electrorheological Fluids. Science, 258, 761-766 (1992). https://doi.org/10.1126/science.258.5083.761

Heris, S.Z., Etemad, S.G., Nasr Esfahany, M. Experimental Investigation of Oxide Nanofluids Laminar Flow Convective Heat Transfer. International Communications in Heat and Mass Transfer, 33, 529-535 (2006). https://doi.org/10.1016/j.icheatmasstransfer.2006.01.005

Heris, S.Z., Nasr Esfahany, M., Etemad, S.G. Experimental Investigation of Convective Heat Transfer of Al2O3/Water Nanofluid in Circular Tube. International Journal of Heat and Fluid Flow, 28, 203-210 (2007). https://doi.org/10.1016/j.ijheatfluidflow.2006.05.001

Heris, S.Z., Nasr Esfahany, M., Etemad, S.G. Investigation of CuO/Water Nanofluid Laminar Convective Heat Transfer Through a Circular Tube. Journal of Enhanced Heat Transfer, 13, 279-289 (2006). https://doi.org/10.1615/JEnhHeatTransf.v13.i4.10

Hwang, K.S., Jang, S.P., Choi, S.U.S. Flow and Convective Heat Transfer Characteristics of Water-based Al2O3 Nanofluids in Fully Developed Laminar Flow Regime. International Journal of Heat and Mass Transfer, 52, 193-199 (2009). https://doi.org/10.1016/j.ijheatmasstransfer.2008.06.032

Joensson, B., Wennerstroem, H., Nilsson, P.G., Linse, P. Self-Diffusion of Small Molecules in Colloidal Systems. Colloid and Polymer Science, 264, 77-88 (1986). https://doi.org/10.1007/BF01410310

Keshishian, N., Nasr Esfahany, M., Etesami, N. Experimental Investigation of Mass Transfer of Active Ions in Silica Nanofluids. International Communications in Heat and Mass Transfer, 46, 148-153 (2013). https://doi.org/10.1016/j.icheatmasstransfer.2013.05.014

Kline, S.J., McClintock, F.A. Describing Uncertainties in Single-sample Experiments. Mechanical Engineering, 75, 3-8 (1953).

Komati, S., Suresh, A.K. CO2 Absorption into Amine Solutions: A Novel Strategy for Intensification Based on the Addition of Ferrofluids. Journal of Chemical Technology and Biotechnology, 83, 1094-1100 (2008). https://doi.org/10.1002/jctb.1871

Laohalertdecha, S., Naphon, P., Wongwises, S. A Review of Electrohydrodynamic Enhancement of Heat Transfer. Renewable and Sustainable Energy Reviews, 11, 858-876 (2007). https://doi.org/10.1016/j.rser.2005.07.002

Lee, J.H., Hwang, K.S., Jane, S.P., Lee, B.H., Kim, J.H. Effective Viscosities and Thermal Conductivities of Aqueous Nanofluids Containing Low Volume Concentration of Al2O3 Nanoparticles. International Journal of Heat and Mass Transfer, 51, 2651-2656 (2008). https://doi.org/10.1016/j.ijheatmasstransfer.2007.10.026

Lee, S., Choi, S.U.S., Li, S., Eastman, J.A. Measuring Thermal Conductivity of Fluids Containing Oxide Nanoparticles. Journal of Heat Transfer, 121, 280-289 (1999). https://doi.org/10.1115/1.2825978

Majazi Dalfard, V. AC Electric Field Deposition Behavior of TiO2 Ceramic Nanoparticles. International Journal of Electrochemical Science, 7, 3299-3305 (2012).

Mansour, R.B., Galanis, N., Nguyen, C.T. Effect of uncertainties in physical properties on forced convection heat transfer with nanofluids. Applied Thermal Engineering, 27, 240-249 (2007). https://doi.org/10.1016/j.applthermaleng.2006.04.011

Modarres, P., Tabrizian, M. Alternating Current Dielectrophoresis of Biomacromolecules: The Interplay of Electrokinetic Effects, Sensors and Actuators B: Chemical, 252, 391-408 (2017). https://doi.org/10.1016/j.snb.2017.05.144

Niu, X.F., Du, K., Xiao, F. Experimental Study on Ammonia-Water Falling Film Absorption in External Magnetic Fields. International Journal of Refrigeration, 33, 686-694 (2010). https://doi.org/10.1016/j.ijrefrig.2009.11.014

Pak, B., Cho, Y.I. Hydrodynamic and Heat Transfer Study of Dispersed Fluids with Submicron Metallic Oxide Particle. Experimental Heat Transfer, 11, 151-170 (1998). https://doi.org/10.1080/08916159808946559

Park, J., Lu, W. Orientation of Core-Shell Nanoparticles in an Electric Field. Applied Physics Letter, 91, 053113 (2007). https://doi.org/10.1063/1.2767191

Ramos, A., Morgan, H., Green, N.G., Castellanos, A. AC Electrokinetics: A Review of Forces in Microelectrode Structure, Journal of Physics D: Applied Physics, 31, 2338-2353 (1998). https://doi.org/10.1088/0022-3727/31/18/021

Rarani, E.M., Etesami, N., Nasr Esfahany, M. Influence of the Uniform Electric Field on Viscosity of Magnetic Nanofluid (Fe3O4/Ethylene Glycol). Journal of Applied Physics, 112, 0949031-0949036 (2012). https://doi.org/10.1063/1.4763469

Reichert, C., Hoell, W.H., Franzreb, M. Mass Transfer Enhancement in Stirred Suspensions of Magnetic Particles by the Use of Alternating Magnetic Fields. Powder Technology, 145, 131-138 (2004). https://doi.org/10.1016/j.powtec.2004.06.010

Sin, M.Y., Shimabukuro, Y., Wong, P.K. Hybrid Electrokinetics for Separation, Mixing, and Concentration of Colloidal Particles. Nanotechnology, 20 (2009). https://doi.org/10.1088/0957-4484/20/16/165701

Suresh, A.K., Bhalerao, S. Rate Intensification of Mass Transfer Process Using Ferrofluids. Indian Journal of Pure and Applied Physics, 40, 172-184 (2001).

Treybal, R.E. Mass transfer operations, McGraw- Hill, New York (2001).

Xuan, Y., Roetzel, W. Conceptions for heat transfer correlation of nanofluid. International Journal of Heat and Mass Transfer, 43, 3701-3707 (2000). https://doi.org/10.1016/S0017-9310(99)00369-5

Xuan, Y., Li, Q. Investigation on Convective Heat Transfer and Flow Features of Nanofluids. Journal of Heat Transfer, 125, 151-155 (2003). https://doi.org/10.1115/1.1532008

Yu, W., Choi, S.U.S. The Role of International Layers in the Enhanced Thermal conductivity of Nanofluids: a Renovated Maxwell Model. Journal of Nanoparticle Research, 5, 167-171 (2003). https://doi.org/10.1023/A:1024438603801